

Supernova Neutrinos, Neutrino Oscillations, and the Mass of the Progenitor Star

Keitaro Takahashi^a, Katsuhiko Sato^{a,b}, Adam Burrows^c and Todd A. Thompson^{d,e}

^a*Department of Physics, University of Tokyo, 7-3-1 Hongo, Bunkyo,
Tokyo 113-0033, Japan*

^b*Research Center for the Early Universe, University of Tokyo,
7-3-1 Hongo, Bunkyo, Tokyo 113-0033, Japan*

^c*Steward Observatory, The University of Arizona,
Tucson, AZ 85721*

^d*Astronomy Department and Theoretical Astrophysics Center, 601 Campbell Hall,
The University of California, Berkeley, CA 94720*

^e *Hubble Fellow*

(March 25, 2022)

We investigate the initial progenitor mass dependence of the early-phase neutrino signal from supernovae taking neutrino oscillations into account. The early-phase analysis has advantages in that it is not affected by the time evolution of the density structure of the star due to shock propagation or whether the remnant is a neutron star or a black hole. The initial mass affects the evolution of the massive star and its presupernova structure, which is important for two reasons when considering the neutrino signal. First, the density profile of the mantle affects the dynamics of neutrino oscillation in supernova. Second, the final iron core structure determines the features of the neutrino burst, i.e., the luminosity and the average energy. We find that both effects are rather small. This is desirable when we try to extract information on neutrino parameters from future supernova-neutrino observations. Although the uncertainty due to the progenitor mass is not small for intermediate θ_{13} ($10^{-5} \lesssim \sin^2 2\theta_{13} \lesssim 10^{-3}$), we can, nevertheless, determine the character of the mass hierarchy and whether θ_{13} is very large or very small.

PACS : 14.60.Pq; 14.60.Lm; 96.40.Tv; 97.60.Bw;

Keywords : Neutrino oscillations; Supernovae;

I. INTRODUCTION

Core-collapse supernovae produce a huge flux of neutrinos of all types. The observation of neutrinos from SN1987A in the Large Magellanic Cloud was a milestone for neutrino astronomy [1,2]. Although some important constraints on neutrino properties were obtained [3–8], the total of 19 events in the Kamiokande and IMB detectors was frustratingly sparse. On the other hand, SuperKamiokande is expected to detect about five to ten thousand neutrinos from the next galactic supernova. Together with the other neutrino detectors arrayed around the world (e.g. SNO, LVD, ICARUS, IceCube), a high-statistics (nearby) supernova will provide an enormous amount of information on both supernova and neutrino properties.

Despite the new oscillation data from solar [9,10], atmospheric [11], reactor [12,13], and accelerator [14] neutrinos, the neutrino mixing angle θ_{13} and the nature of the mass hierarchy re-

main unknown. The constraints and implications of these data have been explored by many authors [15–23]. The greatest uncertainty for the study of neutrino oscillations in the supernova context is the spectral and temporal evolution of the neutrino burst itself. Although the hierarchy of the average energies of the ν_e , $\bar{\nu}_e$, and ν_x neutrinos ($\langle E_{\nu_e} \rangle < \langle E_{\bar{\nu}_e} \rangle < \langle E_{\nu_x} \rangle$) is believed to hold, quantitatively their specific spectra remain a matter of detailed calculation [24,25]. (ν_x denotes ν_μ , ν_τ and their antineutrinos.) Since a supernova is the end-product of a massive star, the properties of the neutrino burst will depend on the properties of the progenitor star, in particular its initial mass and envelope structure [26,27].

In this paper, we study how the initial mass of the progenitor star affects the early neutrino burst and the signature of neutrino oscillations in supernovae. The rest of the paper is organized as follows. In §II, we briefly review the evolution of massive stars, supernova explosions, and neu-

trino bursts. Conversion probabilities for progenitor stars with various masses are calculated and compared in §III. Then, neutrino spectra with and without neutrino oscillations are shown in §IV. Finally in §V we discuss the ramifications of our results and summarize our conclusions.

II. EVOLUTION OF MASSIVE STARS AND SUPERNOVAE

Here, we briefly summarize the evolution of massive stars and supernovae. See [28] for a more extended review.

The evolution and death of a single massive star are determined by its initial mass and metallicity. For the metallicity of the Sun, a star with initial mass below about $8 M_{\odot}$ does not ignite carbon burning and forms a white dwarf. Above about $8 M_{\odot}$, a star completes the advanced burning stages, including for most stars silicon burning. This leads to the presupernova state, which is characterized by a core (iron or NeOMg) of roughly the Chandrasekhar mass surrounded by active burning shells and the accumulated ashes of oxygen, neon, carbon, and/or helium burning. The degenerate core in excess of the Chandrasekhar mass will dynamically collapse and explode as a supernova.

Up to an initial mass of $20 - 25 M_{\odot}$, the supernova leaves behind a neutron star [29,30]. Almost all of the binding energy of the neutron star,

$$E_b \simeq \frac{GM_{\text{NS}}^2}{2R_{\text{NS}}} \simeq 1.5 \times 10^{53} \text{erg} \left(\frac{M_{\text{NS}}}{M_{\odot}} \right)^2 \left(\frac{10 \text{km}}{R_{\text{NS}}} \right), \quad (1)$$

is radiated away as neutrinos. Here G , M_{NS} and R_{NS} are the gravitational constant, the protoneutron star's mass, and its radius, respectively. Due to the differences in interaction strength, average neutrino energies vary with neutrino flavor. A full-scale numerical simulation by the Livermore group [31] using a multi-group flux-limiter diffusion approach for neutrino transport finds $\langle E_{\nu_e} \rangle \simeq 13$ MeV, $\langle E_{\bar{\nu}_e} \rangle \simeq 16$ MeV, $\langle E_{\nu_x} \rangle \simeq 23$ MeV and almost perfect equipartition of the luminosities [32]. Simulations with more sophisticated neutrino transport [33], which are, however, limited to the early phase of neutrino burst, derive a smaller flavor-dependence for the average energy. These differences are essential if neutrino oscillations are to have a perceptible effect on supernova neutrino detection. (For details on supernova neutrinos,

see, for example, the reviews by Burrows [34] and Suzuki [35].)

For progenitor masses larger than $20 - 25 M_{\odot}$, sufficient mass may fall back onto the protoneutron star after explosion to turn it into a black hole. Even in this case, during the early phase which we consider in this paper, the properties of the neutrino burst are almost the same as stated above.

The mass of the progenitor star affects the neutrino oscillation signature of supernova neutrinos through differences in the mantle and core structures. The density profile of the progenitor star, especially of the mantle, is important because it is related to the dynamics of neutrino flavor conversion. On the other hand, the structure of the iron core at the collapse determines the characteristics of the neutrino burst, e.g., the average energy and luminosity for each flavor. We discuss these in the following sections.

III. NEUTRINO FLAVOR CONVERSION AND THE DENSITY PROFILE

The evolution of a massive star is significantly affected by mass loss due to a stellar wind. Indeed, the mass loss can become so strong for a star with initial mass more than about $35 M_{\odot}$ and solar metallicity that the entire hydrogen envelope can be lost prior to the explosion of the star. It is suggested in [28] that the maximum in the final mass is about $20 M_{\odot}$. In addition, the density profile of a star just before the supernova explosion will not depend much on the initial mass of the star. The final density profiles of stars with various initial masses are shown in Fig. 1 [36]. As is expected, they are similar just before collapse.

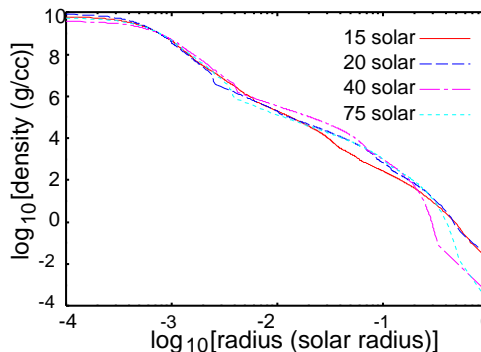


FIG. 1. Density profiles of stars just before supernova explosion with initial mass $15M_{\odot}$, $20M_{\odot}$, $40M_{\odot}$ and $75M_{\odot}$.

The density structure in the range $10\text{g/cc} \lesssim \rho \lesssim 10^4\text{g/cc}$ is particularly important when considering neutrino oscillations. Neutrinos produced in the high-density region of the iron core interact with matter before emerging from the supernova. Due to the non-zero masses and non-zero vacuum mixing angles among various neutrino flavors, flavor conversions can occur in supernovae. When the mixing angle is small, these conversions occur mainly in the resonance layer, where the density is

$$\rho_{\text{res}} \simeq 1.4 \times 10^6 \text{g/cc} \left(\frac{\Delta m^2}{1\text{eV}^2} \right) \left(\frac{10\text{MeV}}{E_{\nu}} \right) \times \left(\frac{0.5}{Y_e} \right) \cos 2\theta. \quad (2)$$

Δm^2 is the mass squared difference, θ is the mixing angle, E_{ν} is the neutrino energy, and Y_e is the mean number of electrons per baryon. Since the inner supernova core is too dense to allow resonance conversion, we focus on two resonance points in the outer supernova envelope. One that occurs at higher density is called the H-resonance and the other, which occurs at lower density, is called the L-resonance. If the mass hierarchy is normal, both resonances occur in the neutrino sector. On the other hand, if the mass hierarchy is inverted, the H-resonance occurs in the antineutrino sector and the L-resonance occurs in the neutrino sector.

The dynamics of conversion including large mixing case is determined by the adiabaticity parameter γ ,

$$\gamma \equiv \frac{\Delta m^2 \sin^2 2\theta}{2E_{\nu} \cos 2\theta} \frac{n_e}{|dn_e/dr|}, \quad (3)$$

which depends on the mixing angle and the mass-squared difference between the involved flavors. In eq. 3, n_e is the electron number density. We define these as:

$$\theta_{13} \text{ and } \Delta m_{13}^2, \text{ at the H - resonance,} \quad (4)$$

and

$$\theta_{12} \text{ and } \Delta m_{12}^2, \text{ at the L - resonance.} \quad (5)$$

Here, the Cabibbo-Kobayashi-Maskawa (CKM) matrix is taken as:

$$U = \begin{pmatrix} c_{12}c_{13} & s_{12}c_{13} & s_{13} \\ -s_{12}c_{23} - c_{12}s_{23}s_{13} & c_{12}c_{23} - s_{12}s_{23}s_{13} & s_{23}c_{13} \\ s_{12}s_{23} - c_{12}c_{23}s_{13} & -c_{12}s_{23} - s_{12}c_{23}s_{13} & c_{23}c_{13} \end{pmatrix}$$

where $s_{ij} = \sin \theta_{ij}$, $c_{ij} = \cos \theta_{ij}$ for $i, j = 1, 2, 3$ ($i < j$). When $\gamma \gg 1$, the resonance is referred to as an ‘adiabatic resonance’ and the fluxes of the two involved mass eigenstates are completely exchanged. However, when $\gamma \ll 1$, the resonance is called ‘nonadiabatic’ and the conversion does not occur. The dynamics of the resonance in supernovae is surveyed by Dighe and Smirnov [15].

The density profile of the star comes into the adiabaticity parameter γ as the scale height $n_e/|dn_e/dr|$. A smaller scale height, that is, a steeper density profile results in less adiabatic resonance. The scale heights of stars with various initial masses, calculated from the density profiles shown in Fig. 1, are given in Fig. 2 as functions of the density. The scale heights vary significantly, but differences between various initial masses are factors of 2 or 3 at the densities relevant for resonances.

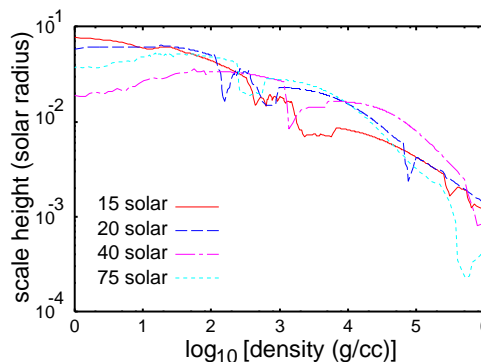


FIG. 2. Scale heights $n_e/|dn_e/dr|$ of stars just before the supernova explosion with initial masses $15 M_{\odot}$, $20 M_{\odot}$, $40 M_{\odot}$, and $75 M_{\odot}$.

To estimate the effects of these differences on neutrino oscillations, we solve numerically the evolution equations for the neutrino wave functions along the density profiles shown in Fig. 1. We take the following values for the neutrino parameters:

$$\sin^2 2\theta_{12} = 0.84, \quad \Delta m_{12}^2 = 7 \times 10^{-5} \text{eV}^2, \\ \sin^2 2\theta_{23} = 1.0, \quad \Delta m_{23}^2 = 3.2 \times 10^{-3} \text{eV}^2. \quad (6)$$

The values of θ_{12} and Δm_{12}^2 are taken from the global analysis of the solar neutrino observations and the KamLAND experiment [37] and correspond to the large mixing angle (LMA) solution of the solar neutrino problem, while those of θ_{23} and Δm_{23}^2 are taken from the analysis of the atmospheric neutrino observations [11]. As for θ_{13} ,

we take $\sin^2 2\theta_{13} = 10^{-4}$. With this θ_{13} , the H-resonance is neither perfectly adiabatic nor non-adiabatic and its adiabaticity is sensitive to the density profile. The normal hierarchy is assumed, but the results are the same for the inverted hierarchy if ν_e is replaced by $\bar{\nu}_e$.

In Fig. 3, the evolution of the probability $P(\nu_e \rightarrow \nu_e)$ that a neutrino emitted as a ν_e at the neutrinosphere remains a ν_e is shown. The neutrino energies on the plot are 5 MeV and 40 MeV. The H-resonance radii and the final probabilities can be quite different for different progenitors and neutrino energies. The observationally important quantity is the final conversion probability and this is shown in Fig. 4 as a function of the neutrino energy. The differences are not so small, about 0.05 – 0.1 at all energies. But if $\sin^2 2\theta_{13}$ is very large or very small, the adiabaticity parameter is very large or very small, respectively. In this case such difference of scale height as in Fig. 2 will not affect the neutrino conversion probability. The range of $\sin^2 2\theta_{13}$ is shown to be $\sin^2 2\theta_{13} \lesssim 10^{-5}$ and $\sin^2 2\theta_{13} \gtrsim 10^{-3}$ in [23].

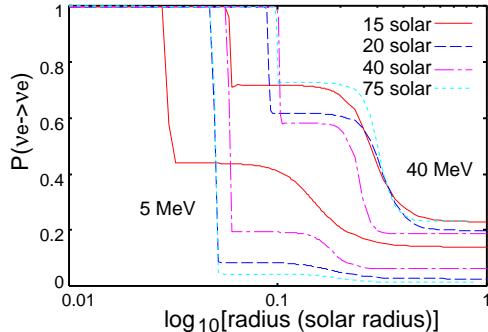


FIG. 3. Evolution of probabilities $P(\nu_e \rightarrow \nu_e)$ that a neutrino emitted as a ν_e at the neutrinosphere remains a ν_e at some radius. Upper and lower curves correspond to neutrino energies of 40 MeV and 5 MeV, respectively.

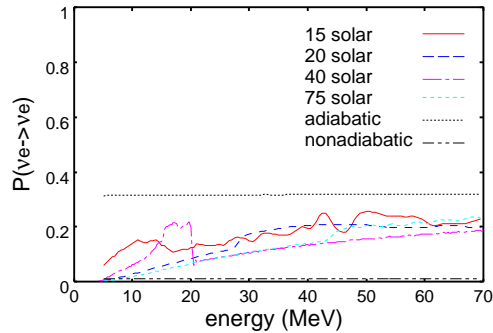


FIG. 4. Energy dependence of probabilities $P(\nu_e \rightarrow \nu_e)$ that a neutrino emitted as a ν_e at the neutrinosphere remains a ν_e at the surface of the star. Also shown are the perfectly adiabatic and non-adiabatic cases for the H-resonance.

Although the density structure evolves as the shock wave propagates, it takes about 2 seconds for the shock wave to reach the H-resonance region [39]. We concentrate our analysis on the early phase when the shock propagation effect can be neglected. The potential time dependence of neutrino oscillations due to shock propagation is discussed by several authors [38,39,17,40].

IV. NEUTRINO BURSTS AND NEUTRINO OSCILLATIONS

As was stated in the previous section, massive stars experience significant mass loss. For current empirical mass loss rates, all solar-metallicity stars initially more massive than about $35 M_\odot$ are thought to become hydrogen-free objects of roughly $5M_\odot$ at the end of their thermonuclear evolution. The corresponding upper limit to the mass of the final iron core is about $2M_\odot$ [28].

The mass of the iron core is determined roughly by the Chandrasekhar mass, which for a zero-temperature, constant Y_e , Newtonian structure is

$$M_{\text{Ch0}} = 5.83Y_e^2 M_\odot. \quad (7)$$

However, there are numerous corrections, some of which are large [41]. To a first approximation, the non-zero entropy of the core is important and

$$M_{\text{Ch}} \sim M_{\text{Ch0}} \left[1 + \left(\frac{s_e}{\pi Y_e} \right)^2 \right], \quad (8)$$

where

$$s_e = 0.50 \left(\frac{\rho}{10^{10} \text{g/cc}} \right)^{-1/3} \left(\frac{Y_e}{0.42} \right)^{2/3} \left(\frac{T}{1 \text{MeV}} \right) \quad (9)$$

is the electronic entropy per baryon. More massive stars have higher entropy and contain larger iron cores on average. However, this general tendency is moderated by the loss and redistribution of entropy that occurs during the late burning stages. Thus, the mass of the iron core as a function of the initial mass will be somewhat uncertain in that a small change in the initial mass results in a large difference in the iron core mass. According to [28], the mass of the iron core is $1.2(1.4) - 1.6M_\odot$ when the initial mass is between $10(20)M_\odot$ and $40M_\odot$. This weak dependence of the iron core mass on the ZAMS progenitor mass leads to a somewhat universal neutrino burst.

Figs. 5-10 show the evolution of the average neutrino energy and number luminosity in the early phase up to 200 milliseconds after bounce. The calculation is based on dynamical models of core-collapse supernovae in one spatial dimension, employing a Boltzmann neutrino radiation transport algorithm, coupled to Newtonian Lagrangean hydrodynamics and a consistent high-density nuclear equation of state. Details of these simulations are described in [33]. As can be seen, the major features of the early neutrino burst are almost independent of the initial mass.

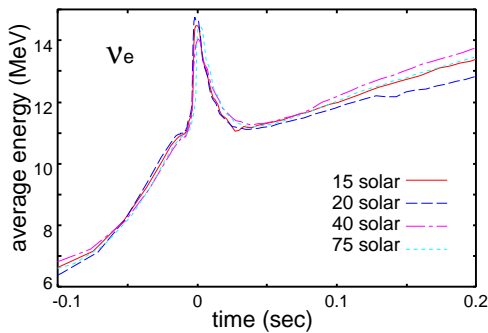


FIG. 5. Evolution of the average ν_e energy of a neutrino burst from a progenitor of initial mass $15M_\odot$, $20M_\odot$, $40M_\odot$ and $75M_\odot$. Time at the bounce is set to zero.

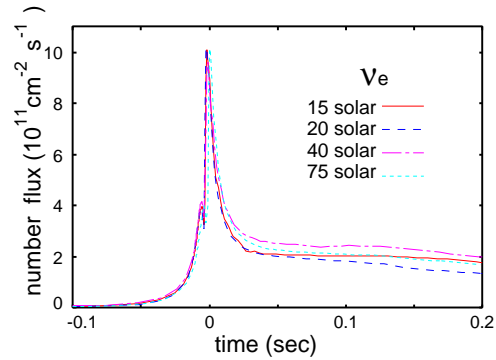


FIG. 6. Evolution of the number flux at the Earth of ν_e neutrinos due to a neutrino burst from a progenitor of initial mass $15M_\odot$, $20M_\odot$, $40M_\odot$ and $75M_\odot$ at a distance of 10 kiloparsecs (kpc). Time at the bounce is set to zero.

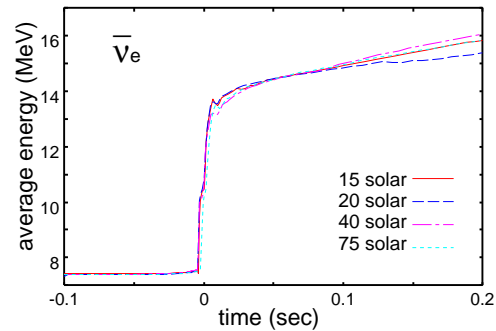


FIG. 7. Same as Fig. 5, but for $\bar{\nu}_e$.

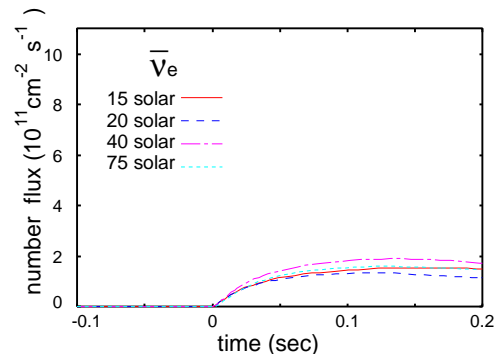


FIG. 8. Same as Fig. 6, but for $\bar{\nu}_e$.

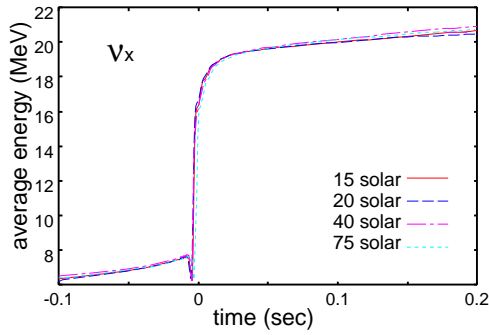


FIG. 9. Same as Fig. 5, but for ν_x .

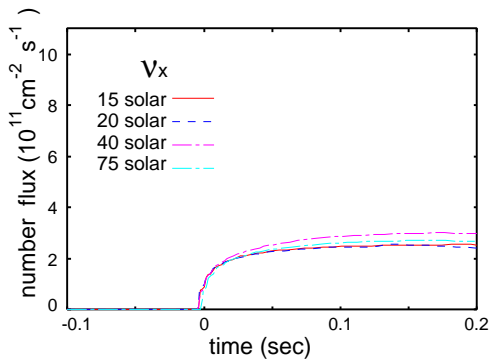


FIG. 10. Same as Fig. 6, but for ν_x .

Combined with the discussion in the previous section, we conclude that the mantle structure and the features of the neutrino burst depend little on the initial mass of the progenitor star if $\sin^2 2\theta_{13} \lesssim 10^{-5}$ or $\sin^2 2\theta_{13} \gtrsim 10^{-3}$. On one hand, this means that we can not easily obtain information about the initial mass from observations of neutrinos during the first 200 milliseconds after bounce. On the other hand, this situation is desirable for extracting information about the neutrino parameters themselves.

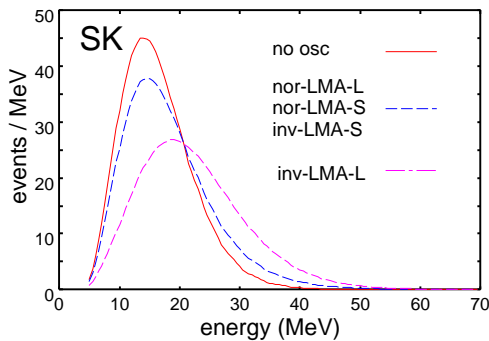


FIG. 11. Time-integrated event spectra at SuperKamiokande using our supernova model with initial mass $20M_{\odot}$ at a distance of 10 kpc.

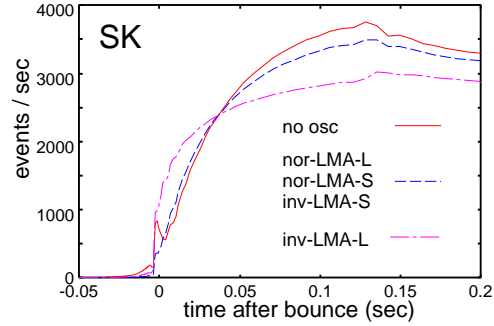


FIG. 12. Time evolution of the event number in SuperKamiokande at a distance of 10 kpc using our supernova model with an initial mass of $20M_{\odot}$.

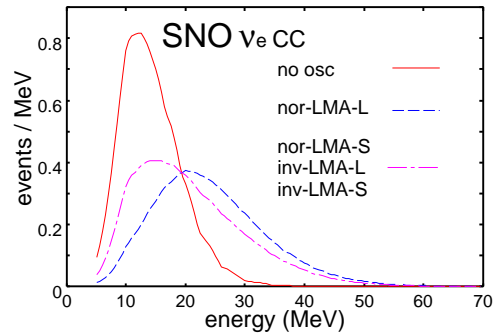


FIG. 13. Time-integrated event spectra at SNO and a distance of 10 kpc using our supernova model with an initial mass of $20M_{\odot}$. Only the charged-current events due to the process $\nu_e + d \rightarrow p + p + e^-$ have been taken into account.

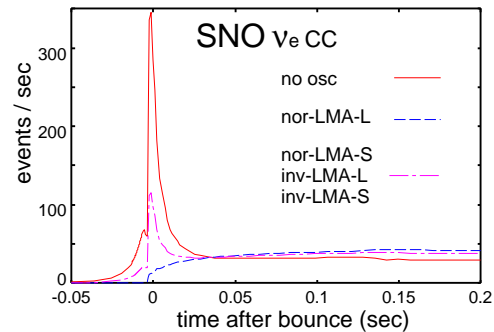


FIG. 14. Time evolution of the event number at SNO and 10 kpc using our supernova model with an initial mass of $20M_{\odot}$. Only the charged-current events due to ν_e ($\nu_e + d \rightarrow p + p + e^-$) absorption have been taken into account.

In our previous papers [20–23], we investigated the possibility of extracting information on neutrino parameters, especially θ_{13} and the neutrino mass hierarchy, from future supernova neutrino observations. We used a numerical supernova model from the Livermore group [31,32] with an initial mass of $15M_{\odot}$. Since the average neutrino energy is flavor dependent ($E_{\nu_e} < E_{\bar{\nu}_e} < E_{\nu_x}$), neutrino oscillations make the spectra of observed ν_e and $\bar{\nu}_e$ neutrinos harder. The extent to which observable neutrinos become harder depends on the adiabaticity parameters at both the H- and L-resonances, which depend on neutrino parameters. We considered models with four sets of neutrino parameters: normal-LMA-L, normal-LMA-S, inverted-LMA-L and inverted-LMA-S. Here, normal-LMA-L means that the mass hierarchy is normal ($m_1^2 < m_2^2 \ll m_3^2$) and θ_{13} is large ($\sin^2 2\theta_{13} = 0.043$), inverted-LMA-S means that the mass hierarchy is inverted ($m_3^2 \ll m_1^2 < m_2^2$) and θ_{13} is small ($\sin^2 2\theta_{13} = 10^{-6}$), and so on. The other parameters are the same as in the previous section.

In Figs. 11–14, we show for a $20M_{\odot}$ progenitor the time-integrated event spectra and the time evolution of the event number at SuperKamiokande (SK) and SNO. The events at SNO include only the charged-current events due to the process $\nu_e + d \rightarrow p + p + e^-$, while all relevant processes are included in the SK event estimates. The detector properties and cross sections used to calculate these events are described in our previous paper [21]. It should be noted that the neutronization burst events at SNO are significantly suppressed due to neutrino oscillation.

In [21,23], we used as a measure of neutrino oscillation the ratio of high-energy event number to low-energy event number at SuperKamiokande, whose events are dominated by $\bar{\nu}_e$, and SNO, which can identify ν_e .

High (low) means higher (lower) than 20 MeV. Our conclusions were that inverted-LMA-L is clearly distinguishable from the other models although the distinction between normal-LMA-L and normal- and inverted-LMA-S is rather difficult. In addition, we determined that normal-LMA-S and inverted-LMA-S are completely degenerate [23]. One of the uncertainties in our analysis was that we did not previously take into account the initial progenitor mass dependence.

We plot in Fig. 15 the above-mentioned event-number ratios for SK (R_{SK}) and SNO (R_{SNO}). Included are results for the above four neutrino parameter models, as well as for the no oscillation case, and various initial progenitor masses. Since we use only early-phase events ($\lesssim 0.2$ sec), the statistical errors are large, whereas in our previous papers we incorporated the full evolution of the neutrino burst based on the simulations of the Livermore group [31,32,26,27]. It can be seen that differences due to initial mass are much smaller than those due to neutrino parameter and statistical errors. Thus, we can conclude that although the uncertainty due to the unknown progenitor mass is not small for intermediate θ_{13} ($10^{-5} \lesssim \sin^2 2\theta_{13} \lesssim 10^{-3}$), we can nevertheless draw conclusions about whether θ_{13} is very large or very small and about the mass hierarchy.

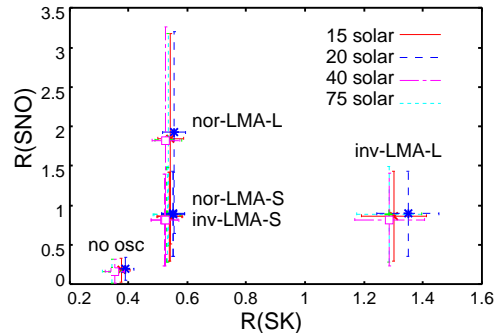


FIG. 15. Plots of R_{SK} and R_{SNO} for the four neutrino parameter models mentioned in the text, as well as for the no oscillation case. Results for various initial progenitor masses are given. The error bars show statistical errors only.

V. DISCUSSION AND SUMMARY

In this paper, we have investigated the initial mass dependence of the early-phase neutrino signal from supernovae. The early-phase analysis has the advantage that it is not affected by the time evolution of the density structure of the star due to shock propagation and is independent of whether the remnant is eventually a neutron star or a black hole. The initial mass does not affect neutrino oscillations in two senses: the density profile of the mantle, which is important for neutrino flavor conversion, and the final iron core structure, which determines the features of the neutrino burst, are almost independent of the initial mass. This is desirable when we try to extract information from fu-

ture supernova-neutrino observations on neutrino parameters. Although the uncertainty due to the progenitor mass is not small for intermediate θ_{13} ($10^{-5} \lesssim \sin^2 2\theta_{13} \lesssim 10^{-3}$), we can nevertheless extract information about whether θ_{13} is very large or very small and about the neutrino mass hierarchy.

VI. ACKNOWLEDGEMENTS

K.T.'s work is supported by Grant-in-Aid for JSPS Fellows. K.S.'s work is supported by Grant-in-Aid for Scientific Research (S) No. 14102004 and Grant-in-Aid for Scientific Research on Priority Areas No. 14079202. A.B. acknowledges support from the Scientific Discovery through Advanced Computing (SciDAC) program of the US DOE, grant number DE-FC02-01ER41184. T.A.T. is supported by NASA through Hubble Fellowship grant #HST-HF-01157.01-A awarded by the Space Telescope Science Institute, which is operated for NASA by the Association of Universities for Research in Astronomy, Inc., under contract NAS 5-26555.

-
- [1] K. Hirata et al., Phys. Rev. Lett. **58**, 1490 (1987).
 - [2] R. M. Bionta et al., Phys. Rev. Lett. **58**, 1494 (1987).
 - [3] J. Arafune and M. Fukugita, Phys. Rev. Lett. **59**, 367 (1987).
 - [4] K. Sato and H. Suzuki, Phys. Rev. Lett. **58**, 2722 (1987).
 - [5] I. Goldman et al., Phys. Rev. Lett. **60**, 1789 (1988).
 - [6] B. Jegerlehner, F. Neubig and G. Raffelt, Phys. Rev. D **54** (1996) 1194.
 - [7] C. Lunardini and A. Yu. Smirnov, Phys. Rev. D **63** (2001) 073009.
 - [8] H. Minakata and H. Nunokawa, Phys. Lett. B **504** 301 (2001).
 - [9] S. Fukuda et al., Phys. Rev. Lett. **86** (2001) 5656.
 - [10] SNO Collaboration, Phys. Rev. Lett. **87** (2001) 071301.
 - [11] Y. Fukuda et al., Phys. Rev. Lett. **82** (1999) 2644.
 - [12] KamLAND Collaboration, K. Eguchi et al., Phys. Rev. Lett. **90** (2003) 021802.
 - [13] M. Apollonio et al., Phys. Lett. B **466** (1999) 415.
 - [14] K2K Collaboration, Phys. Rev. Lett. **90** (2003) 041801.
 - [15] A. S. Dighe and A. Yu. Smirnov, Phys. Rev. D **62** (2000) 033007.
 - [16] G. L. Fogli, E. Lisi, D. Montanino and A. Palazzo, Phys. Rev. D **65** (2002) 073008.
 - [17] C. Lunardini and A. Yu. Smirnov, hep-ph/0302033.
 - [18] A. S. Dighe, M. Th. Keil and G. G. Raffelt, hep-ph/0303210.
 - [19] A. S. Dighe, M. Th. Keil and G. G. Raffelt, hep-ph/0304150.
 - [20] K. Takahashi, M. Watanabe and K. Sato, Phys. Lett. B **510** (2001) 189.
 - [21] K. Takahashi, M. Watanabe, K. Sato and T. Totani, Phys. Rev. D **64** (2001) 093004.
 - [22] K. Takahashi and K. Sato, Phys. Rev. D **66** (2002) 033006.
 - [23] K. Takahashi and K. Sato, Prog. Theo. Phys. in press, hep-ph/0205070.
 - [24] G. G. Raffelt, Astrophys. J. **561** (2001) 890.
 - [25] G. G. Raffelt, M. Th. Keil, R. Buras, H. -T. Janka and M. Rampp, Proc. NOON 03 (10-14 February 2003, Kanazawa, Japan), astro-ph/0303226.
 - [26] R. Mayle, Ph. D. Thesis, University of California (1987).
 - [27] R. Mayle, J. R. Wilson, and D. N. Schramm, Astrophys. J. **318** (1987) 288.
 - [28] S. E. Woosley, A. Heger and T. A. Weaver, Rev. Mod. Phys. **74** (2002) 1015.
 - [29] C. L. Fryer, Astrophys. J. **522** (1999) 413.
 - [30] C. L. Fryer and V. Kalogera, Astrophys. J. **554** (2001) 548.
 - [31] J. R. Wilson, R. Mayle, S. Woosley, T. Weaver, Ann. NY Acad. Sci. **470**, 267 (1986).
 - [32] T. Totani, K. Sato, H. E. Dalhed and J. R. Wilson, Astrophys. J. **496** (1998) 216.
 - [33] T. A. Thompson, A. Burrows, and P. A. Pinto, Astrophys. J. **592**, July 20, 2003 (astro-ph/0211194).
 - [34] A. Burrows, Ann. Rev. Nuc. Part. Sci. **40** (1990) 181.
 - [35] H. Suzuki: Supernova Neutrino in *Physics and Astrophysics of Neutrino*, edited by M. Fukugita and A. Suzuki (Springer-Verlag, Tokyo, 1994).
 - [36] SciDAC Supernova Science Center homepage: <http://www.supersci.org/>
 - [37] J. N. Bahcall, M. C. Gonzalez-Garcia and C. Pena-Garay, JHEP **02** (2003) 009.
 - [38] R. C. Schirato and G. M. Fuller, astro-ph/0205390.
 - [39] K. Takahashi, K. Sato, H. E. Dalhed and J. R. Wilson, astro-ph/0212195.
 - [40] G. L. Fogli, E. Lisi, A. Mirizzi and D. Montanino, hep-ph/0304056.
 - [41] F. X. Timmes, S. E. Woosley and T. A. Weaver, Astrophys. J. **457** (1996) 834.